NANO LETTERS

Letter

pubs.acs.org/NanoLett

Raman Enhancement Effect on Two-Dimensional Layered Materials: Graphene, h-BN and MoS_2

Xi Ling,*[,†] Wenjing Fang,[†] Yi-Hsien Lee,[†,∥] Paulo T. Araujo,[‡,⊥] Xu Zhang,[†] Joaquin F. Rodriguez-Nieva,[‡] Yuxuan Lin,[†] Jin Zhang,[§] Jing Kong,[†] and Mildred S. Dresselhaus*[,†,‡]

[†]Department of Electrical Engineering and Computer Science and [‡]Department of Physics, Massachusetts Institute of Technology, Cambridge, Massachusetts 02139, United States

[§]Center for Nanochemistry, Beijing National Laboratory for Molecular Sciences, Key Laboratory for the Physics and Chemistry of Nanodevices, State Key Laboratory for Structural Chemistry of Unstable and Stable Species, College of Chemistry and Molecular Engineering, Peking University, Beijing 100871, People's Republic of China

[∥]Material Sciences and Engineering, National Tsing-Hua University, Hsinchu, 30013, Taiwan

[⊥]Department of Physics and Astronomy, University of Alabama, Tuscaloosa, Alabama 35487, United States

Supporting Information

ABSTRACT: Realizing Raman enhancement on a flat surface has become increasingly attractive after the discovery of graphene-enhanced Raman scattering (GERS). Two-dimensional (2D) layered materials, exhibiting a flat surface without dangling bonds, were thought to be strong candidates for both fundamental studies of this Raman enhancement effect and its extension to meet practical applications requirements. Here, we study the Raman enhancement effect on graphene, hexagonal boron nitride (h-BN), and molybdenum disulfide (MoS_2), by using the copper phthalocyanine (CuPc) molecule as a probe. This molecule can sit on these layered materials in a face-on configuration. However, it is found that the Raman enhancement effect, which is observable on graphene, hBN, and MoS_2, has different enhancement factors for the different vibrational modes of CuPc, depending strongly on the surfaces. Higher-frequency phonon modes of CuPc (such as those at 1342, 1452, 1531 cm^{-1}) are enhanced more strongly on graphene than that on h-BN, while the lower frequency phonon modes of CuPc (such as those at 682, 749, 1142, 1185 cm^{-1}) are enhanced more strongly on h-BN than that on graphene. MoS_2 demonstrated the weakest Raman enhancement effect as a substrate among these three 2D materials. These differences are attributed to the different enhancement mechanisms related to the different electronic properties and chemical bonds exhibited by the three substrates: (1) graphene is zero-gap semiconductor and has a nonpolar C−C bond, which induces charge transfer (2) h-BN is insulating and has a strong B−N bond, while (3) MoS_2 is semiconducting with the sulfur atoms on the surface and has a polar covalent bond (Mo−S) with the polarity in the vertical direction to the surface. Therefore, the different Raman enhancement mechanisms differ for each material: (1) charge transfer may occur for graphene; (2) strong dipole−dipole coupling may occur for h-BN, and (3) both charge transfer and dipole−dipole coupling may occur, although weaker in magnitude, for MoS_2. Consequently, this work studied the origin of the Raman enhancement (specifically, chemical enhancement) and identifies h-BN and MoS_2 as two different types of 2D materials with potential for use as Raman enhancement substrates.

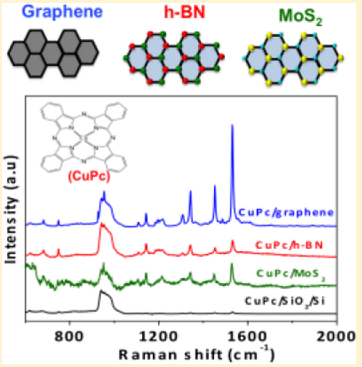

KEYWORDS: *Raman enhancement, two-dimensional materials, chemical mechanism, charge transfer, dipole−dipole interaction*

The Raman enhancement effect is an attractive phenomenon for fundamental studies of both light-matter and matter−matter interactions and also for microanalytical applications.[1] Among the numerous Raman enhancement techniques,[2−5] surface-enhanced Raman scattering (SERS) has been most intensively studied but there still remains many ambiguities regarding the pertinent enhancement mechanisms.[6−10] For instance, the two most widely accepted mechanisms for the SERS effect are (1) the enhancement of the local electromagnetic fields around metallic structures,[6] called the electromagnetic mechanism (EM), which is clearly explained by theoretical and experimental studies, and (2) the chemical interaction between the absorbate and the substrate,[10] called the chemical mechanism (CM), which is poorly understood, because it is an effect of smaller magnitude than the EM effect and it is usually covered up by the EM effect. No matter which kind of mechanism is operative, the substrate is obviously pivotal for the observation of SERS enhancement. In the past, noble metals have been dominant as the substrate material for SERS because of the huge enhancement factors

Received: December 12, 2013
Revised: April 18, 2014
Published: April 24, 2014

they induced through the EM effect.[4,6] However, there are some disadvantages associated with a metal substrate, such as side-reactions of the adsorbate due to the catalytic effect of metals, the deformation of the adsorbate due to the strong metal−adsorbate interaction, and the strong spectral background because of the carbonization effect on the metal, which are also some reasons why SERS has not been widely explored in practical applications.[11] Therefore, exploring nonmetallic materials as a substrate, which were previously considered not to be suitable as an active SERS mediator, for Raman enhancement could become significant in overcoming the disadvantages of metal substrates.[11−14] At this time, the graphene surfaces has made the most important impact on the discovery of graphene-enhanced Raman scattering (GERS) effect,[15] which was proved to be an attractive signal enhancement technique that yields clean, uniform, and repeatable Raman-enhanced signals. Monolayer graphene has already been shown to be an effective Raman enhancement substrate, having many advantages.[15,16] The intriguing prospects of graphene as a Raman enhancement substrate include (1) convenient control of molecular orientation, because molecular orientation is an important but challenging topic in traditional SERS studies;[17] (2) easy to combine with a traditional metallic substrate, which allows us to take advantage of both metal substrates and two-dimensional (2D) material substrates;[18−21] (3) suitable as a flexible substrate, which is desirable for some specific applications, such as the detection of food additives;[11] and (4) dominated by the chemical mechanism rather than the electromagnetic mechanism, even though the Raman enhancement factor is not as dramatic as that on the metal substrate,[17,22−27] which offers an ideal environment for the deep study of the chemical mechanism. It has been realized that developing a flat surface for Raman enhancement has promising importance for the further application of SERS. Most two-dimensional (2D) materials provide a good choice as an ideal flat substrate.

In the present work, diverse 2D materials beyond graphene are adopted to study Raman enhancement on different types of 2D material surfaces. Copper phthalocyanine (CuPc) is used here as a probe molecule as in our previous work,[17] because of its strong Raman scattering and negligible disturbance by the PL background, thereby allowing us to directly observe the enhancement effect of individual molecules.[28] Hexagonal boron nitride (h-BN)[29] and the transition metal dichalcogenides (TMD) (e.g., molybdenum disulfide (MoS_2)),[30] two typical prototype 2D materials, were highlighted and have been widely studied. Both have a structure somewhat similar to graphene but different electronic properties as well as different surface chemical properties. The comparison of the enhancement effect among the three different 2D materials will be helpful to further investigate the chemical enhancement effect. Because there are no dangling bonds on the surface of these 2D layered materials, the interaction between CuPc and these 2D materials mainly results from a van der Waals interaction and free from direct chemical bonding.[31,32] Specifically, two main kinds of interactions between CuPc and these 2D materials should be considered. One is the charge transfer interaction, and another one is the dipole−dipole interaction. For graphene, which is semiconducting with a zero-bandgap and is nonpolar,[33,34] the charge transfer interaction with the CuPc molecule is strong because of the metallic character of graphene. However, the dipole−dipole interaction between CuPc and graphene is small due to its nonpolar signature. In contrast, for h-BN, which is highly polar and insulating with a large band gap of 5.9 eV,[29,35] the interface dipole interaction is strong and dominant, but h-BN has negligible charge transfer interaction. In the case of MoS_2, which is semiconducting and is a less polar material in comparison to h-BN (because MoS_2 is a three atomic layer structure with sulfur on both outside layers and Mo in the center layer),[36] both the charge transfer and dipole−dipole interactions are weak.[32] By analyzing the enhancement effect of these three representative 2D materials, the origin of the enhancement mechanism in these systems is investigated and a deeper understanding on the overall Raman enhancement effect has been achieved.

Results and Discussion. Figure 1 provides the schematic structures and sample assembly information used for the three

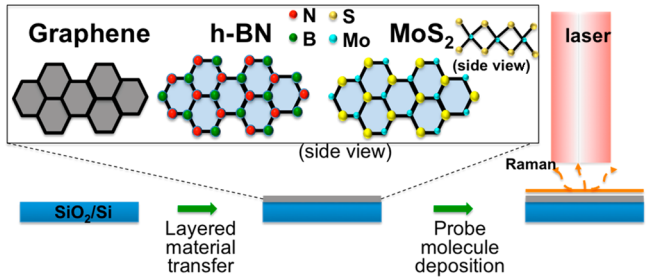

Figure 1. Schematic illustration of the sample preparation and measurement procedure. The inset shows the top view structures of graphene, h-BN, and MoS_2. The layered material substrate below the inset is shown in gray and the probe molecule is shown on the right in red in the assembled sample.

2D materials. First, graphene, h-BN, or MoS_2 was transferred onto a 300 nm SiO_2/Si substrate. Then, copper phthalocynine (CuPc) molecules, used as a Raman probe, were deposited in a batch on the above substrates by vacuum thermal evaporation. Because the GERS effect is a first layer effect,[22] a submonolayer coverage of the CuPc molecules (2−4 Å thick) was deposited on the substrate. The full XPS (X-ray photoelectron spectroscopy) spectra of the CuPc molecule on the surface of graphene (black), h-BN (red), and MoS_2 (blue) are shown in Figure S1 of the Supporting Information, allowing us to determine the electronic state of the atoms associated with both the CuPc molecule and the corresponding 2D materials.[32] The assignments of the XPS signals are shown in Table S1 in the Supporting Information. Specifically, the detailed XPS spectra of Cu 2p3/2, N 1s and C 1s are shown in Figure 2a−c. From Figure 2a, we see that the intensity of the Cu 2p3/2 signal at around 934 eV on graphene, h-BN, and MoS_2 is similar, which indicates that the density of CuPc molecules is almost equal on all the substrates. For the C 1s signal in Figure 2c, the integrated intensity on graphene is more than twice stronger than that on h-BN and MoS_2. It is attributed to the carbon in graphene, which also contributes to the C 1s signal. This result also indicates that the thickness of the observed CuPc molecules is a submonolayer. In more detail (Figure 2c), the C 1s signal on graphene is fitted by two peaks, where one at 283.4 eV is attributed to the carbon from graphene, and the other one at 284.2 eV is attributed to the carbon from CuPc. For the 284.2 eV peak, it has nearly the same intensity as the CuPc signals on h-BN and on MoS_2, which further indicates that the density of CuPc molecules is nearly equal on all of the above 2D materials. For a similar reason, the intensity for the N 1s signal on h-BN in Figure 2b is stronger than that on

dx.doi.org/10.1021/nl404610c | Nano Lett. 2014, 14, 3033−3040

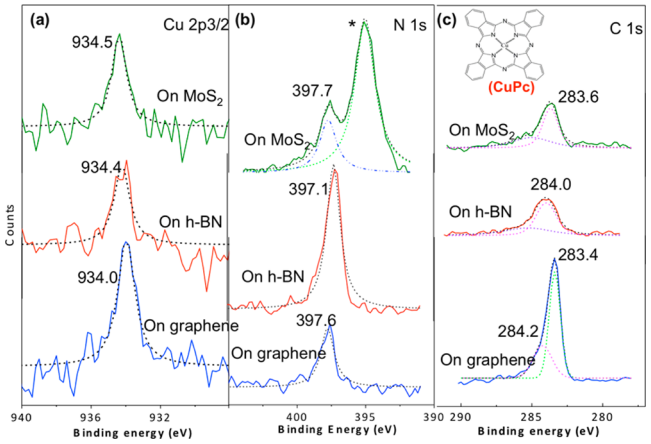

Figure 2. Well-resolved XPS spectra of Cu 2p3/2 (a), N 1s (b), and C 1s (c) of the CuPc molecule on top of a graphene (blue), h-BN (red), and MoS_2 (green) surface. The peak marked by "*" in the green line of (b) is from the electron state of the Mo 2p3/2 orbit. The inset in (c) shows the chemical structure of the CuPc molecule.

graphene and on MoS_2. Therefore, the XPS result shows that the same amount of submonlayer CuPc molecules was deposited on the graphene, h-BN, and MoS_2 substrates.

To compare the enhancement effect of CuPc molecules on graphene, h-BN, and MoS_2 surface, the Raman spectra were collected on the representative samples using the resonant excitation wavelength (632.8 nm) of the CuPc molecule as the laser excitation wavelength, as shown in Figure 3. On the blank

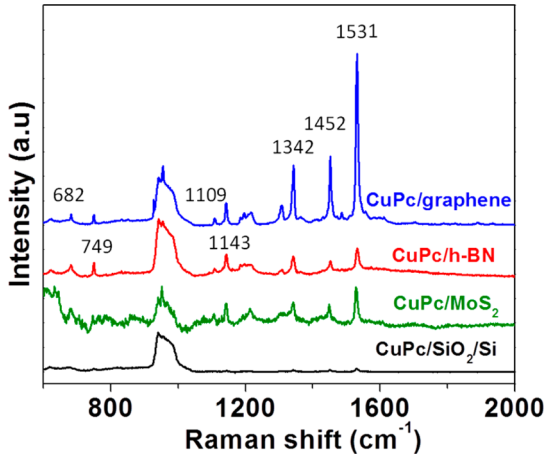

Figure 3. Raman spectra of the CuPc (2 Å) molecule on the blank SiO_2/Si substrate (black line), on graphene (blue line), on h-BN (red line), and on MoS_2 (green line) substrates. The Raman signal was excited by a 632.8 nm laser. The numbers marked on the peaks are the peak frequencies of the Raman signals from the CuPc molecule. For all of the spectra, the baseline correction was removed to have better comparison.

SiO_2/Si substrate, the Raman signals of CuPc are negligible, as shown by the black curve in Figure 3. With a careful analysis, only some vibrational modes with large polarizability,[37] such as the 1531, 1450, and 1340 cm^{-1} modes, can be clearly observed. However, on graphene, h-BN, and MoS_2 substrates, the Raman signals of CuPc are enhanced by different factors. Among them, the enhancement on graphene and h-BN is very strong. On MoS_2, due to the background of the photoluminescence of the MoS_2 (see Figure S2 in Supporting Information) the Raman signals of CuPc are partly covered up and less evident in comparison to the signals on graphene and h-BN. Nevertheless, after the baseline correction of the spectra, from some of the peaks in the range of 1300−1600 cm^{-1}, the spectrum indicates that the Raman enhancement effect on MoS_2 is close to that on h-BN. For the low-frequency Raman signals of CuPc, we do not observe them on MoS_2, which is probably due to the disturbance of the photoluminescence background or the weak enhancement effect. The enhancement factors can be calculated by comparing the Raman intensity on the 2D materials with that on the blank SiO_2/Si substrate. Taking the 1531 cm^{-1} mode as an example, the enhancement factor is about 63, 13, and 16 on graphene, h-BN, and MoS_2, respectively. The enhancement phenomenon on these layered 2D materials is further confirmed by using the NAA (4′-nitrobenzene-diazoaminoazobenzene) molecule as a probe and the 532.5 nm laser line as the excitation wavelength (see Part 3 in the Supporting Information). To exclude the influence of the underneath substrate on the Raman intensity, further experiments were carried out on suspended graphene and on suspended h-BN. The suspended structures were prepared by transferring chemical vapor deposition (CVD) graphene and h-BN on to a transmission electron microscopy (TEM) grid with holes of 3 μm in diameter. In the atomic force microscopy (AFM) image shown in Figure 4a−d, the graphene (a,b) and h-BN (c,d) were successfully suspended on the holes. Figure 4e shows a comparison of the Raman spectra of the CuPc molecule on suspended graphene, suspended h-BN, and the SiO_2/Si substrate. The enhancement effects are similar to that shown in Figure 3, which suggests that the enhancement effect is an intrinsic property of these 2D materials, but independent of the underneath SiO_2/Si substrates.

Table 1 listed the spectral parameters obtained by fitting the peaks with Lorentzian line shapes. It is also clear that the enhancement factors for different vibrational modes are significantly different between graphene and h-BN. For example, the enhancement factors vary over a wide range from several times to several tens of times due to the selection rules of the chemical enhancement effect.[28] The largest enhancement of a vibrational mode of the CuPc molecule on graphene occurs for the 1531 cm^{-1} mode, which is enhanced by about 63 times; while on h-BN, the largest enhanced vibrational mode is at 1143 cm^{-1}, which is enhanced about 41 times. Moreover, for the vibrational modes located at high frequency (such as 1342, 1452, 1531 cm^{-1}), the enhancement is stronger on graphene than that on h-BN; for the vibrational modes located at lower frequency (such as 682, 749, 1143, 1196 cm^{-1}), the enhancement is stronger on h-BN than that on graphene. For the vibrational modes for the CuPc molecule,[38−40] the low-frequency vibrations are mostly assigned to the breathing vibration of the macro ring, and the high-frequency vibrations are mostly related with the stretching or bending vibration of the isoindole ring. The results in Figure 3 indicate that the interaction mechanism between CuPc/graphene and h-BN/graphene is different, which will be analyzed later in this paper. In addition, we did not observe an obvious difference in the Raman shift of the vibrational modes of the CuPc molecule on graphene and h-BN relative to that on SiO_2/Si substrate, even though such differences are reported for some other probe molecules in the references.[41,42] This may result from a relatively weak physical interaction between the planar structure of the CuPc molecule[43] and the

dx.doi.org/10.1021/nl404610c | Nano Lett. 2014, 14, 3033−3040

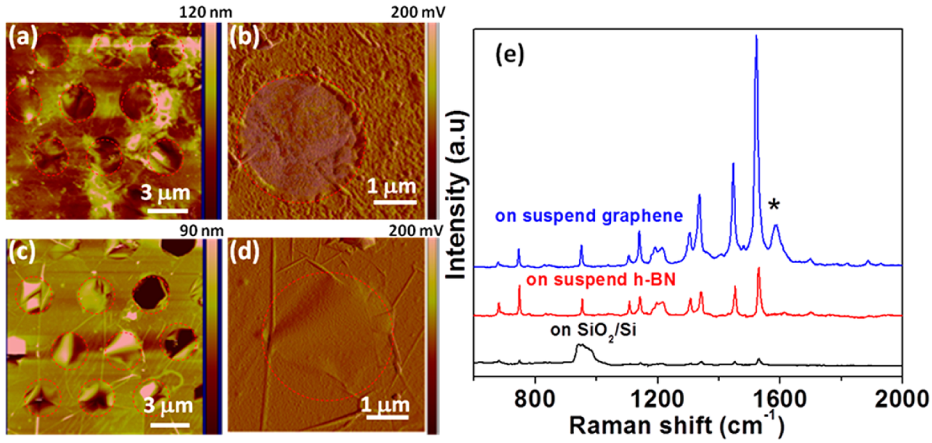

Figure 4. (a,b) The AFM height image (a) and the amplified (b) image of suspended graphene on a TEM grid. (c,d) The AFM height image (c) and amplified (d) image of suspended BN on a TEM grid. (e) Comparison of the Raman spectra of the 4 Å CuPc molecule on a blank SiO_2/Si (black line), on suspended h-BN (red line), and on suspended graphene (blue line) substrates. The baseline correction of the spectra are removed for better display.

Table 1. Intensity Comparison of the CuPc Raman Vibrational Modes on Different Substrates[a]

ω_G (cm^{-1})	$\omega_{h\text{-}BN}$ (cm^{-1})	$I_{SiO2/Si}$	I_G	$I_{h\text{-}BN}$	EF_G	$EF_{h\text{-}BN}$	$EF_G/EF_{h\text{-}BN}$	mode assignment
682.1	682.2		291.5	697.3			0.4	B_{1g}, in plane full symmetric nonmetal bound N−M stretch and outer ring stretches
749.2	749.3	75.4	398.9	1007.6	5.2	13.3	0.4	B_{2g}, in plane ring symmetric N−M stretch
832.6	832.5		56.8	182.4			0.3	A_{1g}, in plane full symmetric N−M stretch
1109.0	1108.7	20.2	257.9	329.8	12.7	16.3	0.8	A_{1g}, in plane symmetric N−M−N bend
1142.9	1143.2	44.7	912.0	1834.7	20.3	41.0	0.5	B_{2g}, in plane ring symmetric and outer rings breathing
1196.1	1196.7	24.36	425.3	720.4	17.4	29.5	0.6	B_{1g}, in plane symmetric N−M−N bend
1207.4	1214.7		274.8	364.0			0.7	A_{2g}
1217.6	1221.2	23.2	402.2	190.2	17.2	8.1	2.1	B_{2g}
1306.6	1305.7	29.4	713.0	205.9	24.2	6.9	3.4	B_{2g}, in plane symmetric outer ring rotation
1342.0	1341.6	62.8	2331.6	1315.4	37.1	20.9	1.7	B_{1g}, in plane full symmetric N−C stretch and ring C−C stretch
1452.1	1452.1	61.1	2606.9	590.7	42.6	9.6	4.4	B_{2g}, in plane ring symmetric outer ring C−C stretch
1531.2	1532.1	106.2	6752.1	1405.8	63.5	13.2	4.8	B_{2g}, ring C−C stretch and in plane ring symmetric non metal bound N−C stretch

[a] ω_G: Raman shift of the CuPc molecule on Graphene. $\omega_{h\text{-}BN}$: Raman shift of the CuPc molecule on h-BN. $I_{SiO2/Si}$: Raman intensity of CuPc molecule on a blank SiO_2/Si substrate. I_G: Raman intensity of CuPc molecule on graphene. $I_{h\text{-}BN}$: Raman intensity of CuPc molecule on h-BN. EF_G: Intensity ratio of the Raman signal of CuPc molecule on graphene and on a blank SiO_2/Si substrate. $EF_{h\text{-}BN}$: Intensity ratio of the Raman signal of CuPc molecule on h-BN and on a blank SiO_2/Si substrate.

2D materials, where the deformation of the molecule due to the surface interaction is negligible.

In addition, in the previous work[25] we reported the thickness dependence of the enhancement on graphene. We found that the enhancement factors slightly decrease with an increase in the graphene layer number due to the 2.3% absorption of the incident laser light per graphene layer.[44,45] In contrast, the enhancement factors for different thicknesses of h-BN are the same because h-BN is highly transparent in the visible range. As shown in Figure 5a, an h-BN flake with different thicknesses was obtained by mechanical exfoliation. The thickness of the regions "1" to "5" is roughly estimated from the color of the flakes, as seen in the optical image shown in the inset of Figure 5a. The typical Raman peak at 1367 cm^{-1} from h-BN was marked by the shadow in Figure 5a. The intensity of the 1367 cm^{-1} peak increases from spectra 1 to 5 (where the spectrum 0 is collected on a CuPc/SiO_2/Si sample without h-BN), further indicating the increase of the thickness of h-BN in going from 1 to 5. Nevertheless, the intensity of the Raman signals from the CuPc molecule is not dependent on the h-BN thickness. That is to say, the enhancement effect observed is uniform over both the thick h-BN and the thin h-BN regions (shown in spectra 1−5 in Figure 5a), which is different from the results on graphene (Figure 5 in ref 15). Furthermore, Raman mappings of the intensity of the 1531 cm^{-1} mode from the CuPc molecule (Figure 5c,e) were carried out on the flakes in Figure 5b,d, respectively. The result shows that the enhancement factor does not depend on the h-BN thickness, because the distribution of the intensity is uniform no matter how thick is the h-BN flake. This result suggests that h-BN is a superior substrate regarding uniformity, when compared to graphene.

Graphene and h-BN are two typical systems for understanding the chemical mechanism of the Raman enhancement, because of their similar structure but different electronic properties. To understand the similarities and differences of the enhancement effect on graphene and on h-BN, we propose the following mechanisms for the Raman enhancement on the h-BN and graphene substrates. One is the charge transfer interaction with CuPc; the other one is the enhanced interface dipole−dipole interaction from the 2D materials. Because h-BN is a wide bandgap insulator, the EM can be ruled out as the dominant excitation mechanism, because the EM originates

dx.doi.org/10.1021/nl404610c | Nano Lett. 2014, 14, 3033−3040

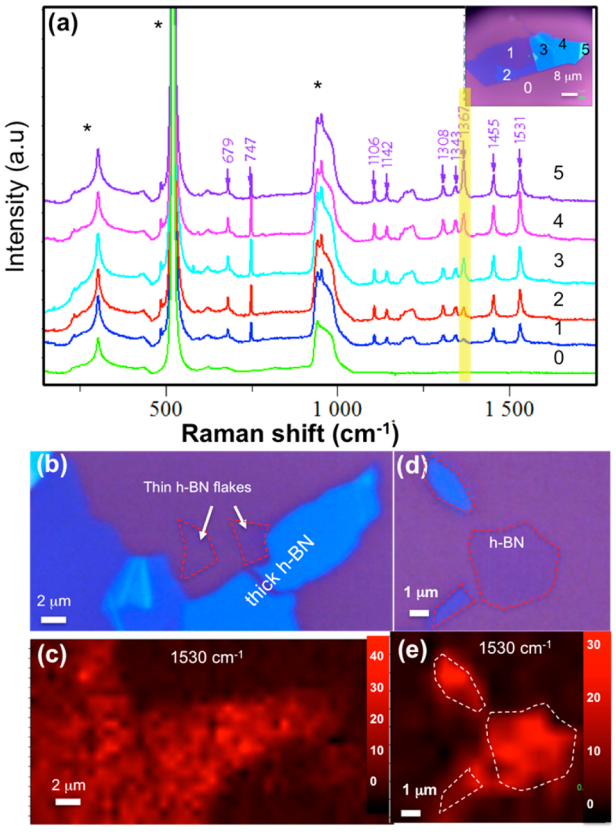

Figure 5. (a) The Raman enhancement effect on h-BN flakes of different thickness. The inset shows the mechanically exfoliated flake with different thicknesses of h-BN. The numbers 0, 1, 2, 3, 4, and 5 in the inset and labels on the traces correspond to the position where the Raman spectra were collected. The "*" marked peaks are from the SiO_2/Si substrate. The yellow shadow shows the location of the 1367 cm^{-1} Raman mode from h-BN. (b,d) The optical images of two h-BN flakes. Some h-BN flakes are marked by arrows or by a red dashed ring. (c,e) The Raman mapping images for the CuPc vibrational mode at 1531 cm^{-1} corresponding to (b,d), respectively.

from the surface plasmon resonance, which is the property of a metal.[6] Also, we exclude the electromagnetic mechanism for the enhancement effect on graphene because no surface plasmon is observed when using visible laser wavelengths.[46] Moreover, recently, Hao's results by electric and chemical doping also support the chemical mechanism exclusively.[24] Considering the properties of graphene first, the contact of the CuPc molecule with graphene can increase the electron transition probability by increasing the electron density of states, because graphene is a zero-gap semiconductor with numerous available electron states at around the HOMO (highest-occupied molecular orbital) and the LUMO (lowest-unoccupied molecular orbital) levels of the CuPc molecule.[47,48] Meanwhile, graphene is nonpolar, so that the dipole−dipole interaction between graphene and CuPc is small. In contrast, the electron density of states of h-BN has less influence on the increase of the electron transition probability due to the large band gap. However, h-BN has a polar structure, which can induce an interface dipole interaction with the CuPc molecule. According to Fermi's golden rule, the electron transition probability rate can be expressed as

$$w_{lk} = \frac{2\pi}{\hbar} g(E_k) |H'_{kl}|^2 \quad (1)$$

where the $g(E_k)$ is the density of states and H'_{kl} is the matrix element for the LUMO−HOMO transition. The interface dipole interaction in h-BN will result in a local symmetry-related perturbation, which can increase the matrix element H'_{kl} in eq 1. According to the above analysis, we conclude that both graphene and h-BN can induce an increase of the electron transition probability of the CuPc molecule for different reasons, where on graphene the transition originates from the charge transfer interaction with CuPc, which has been reported in our previous work as a ground state charge transfer.[26] On h-BN, it originates from the interface dipole interaction with the CuPc molecule induced by the highly polar B−N bond, which results in a symmetry-related perturbation in the CuPc molecule.

This assumption is further supported by the UV−vis absorption spectra of the CuPc molecule on these 2D materials. Figure 6 shows the UV−vis absorption spectra of graphene (black line), h-BN (red line), and MoS_2 (blue line) before (a) and after (b) the CuPc molecule deposition. In Figure 6a, we can see the typical absorption peak of graphene at 270 nm, h-BN at 202 nm, and MoS_2 at 430, 621, and 670 nm. After the deposition of the CuPc molecules, the absorption peaks of the 2D materials remain the same. An additional peak appears on the spectrum at around 700 nm, which is assigned to the Q-band absorption of the CuPc molecule (though the peak in the blue line is overlapped with the absorption peak at 670 nm of the MoS_2 itself, we can still observe an obvious shoulder peak

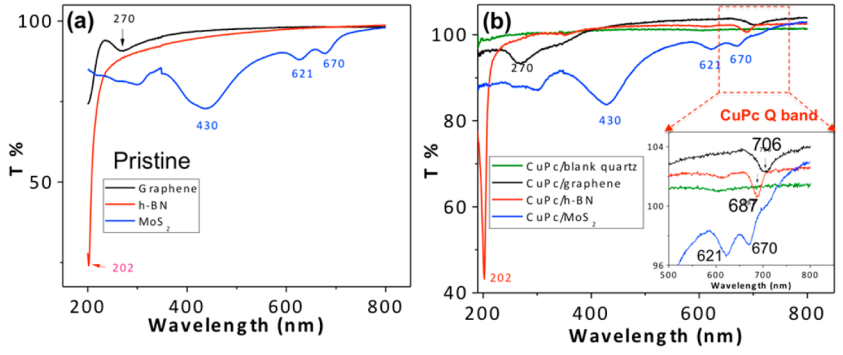

Figure 6. (a) The UV−vis transmission spectra of pristine graphene (black curve), h-BN (red curve), and MoS_2 (blue curve) substrates. (b) The UV−vis absorption spectra of the 4 Å CuPc molecule on graphene (black curve), h-BN (red curve), and MoS_2 (blue curve) substrates. The green curve in (b) is the UV−vis absorption curve for the pristine CuPc molecule without 2D materials underneath. The inset in (b) is the zoom-in spectra in the wavelength range from 500 to 800 nm.

dx.doi.org/10.1021/nl404610c | Nano Lett. 2014, 14, 3033−3040

beside it, which is contributing to the absorption of the CuPc molecule).[49,50] It is worth mentioning that if there were no 2D materials underneath the molecule, the absorption peak for the same amount of CuPc would be invisible (the green line in Figure 6 b). The enhancement of the absorption by the substrate indicates that the electron transition probability is increased by the substrate, as compared to the background. Moreover, the absorption peak position of the CuPc molecule on graphene and on h-BN is different. It is 706 nm for graphene and 687 nm for h-BN (see the inset of Figure 6b). Here, the observation of just a small perturbation in the absorption spectrum of MoS_2 caused by the presence of the CuPc molecule on MoS_2 provides further evidence that MoS_2 is a substrate with a weak charge transfer mechanism and a weak dipole−dipole interaction. Compared with the intrinsic absorption of the CuPc molecule on the quartz substrate without the 2D materials, where the Q-band absorption peak splits into two peaks located at 626 and 700 nm (see Figure S4 in the Supporting Information), the absorption peak of the CuPc molecule is shifted when the molecule is on graphene or h-BN. Because the monomeric CuPc species is dominant in this system, the absorption peak of CuPc in Figure 6b corresponds to the absorption band of the pristine CuPc molecule at 700 nm.[17] Therefore, the redshift of the CuPc absorption on graphene indicates the enlargement of the conjugated structure of CuPc,[51,52] which is consistent with the contribution from the charge transfer interaction between the CuPc molecule and graphene. On h-BN, the blueshift of the absorption is attributed to the dipole interaction in the polar environment.[53,54] On the basis of this difference in mechanisms, the enhancement factors on a graphene substrate become larger and larger with the increase of the frequency of the vibrational mode, since the larger the frequency of the vibrational mode, the more easily the charge transfer happens; however, on h-BN the vibration with a larger dipole will be enhanced more. It is for these various reasons why the 1143 cm^{-1} vibrational mode is enhanced the most on h-BN (see Table 1).[37,55]

Conclusions. In this study, we investigated the Raman enhancement effect of the CuPc molecule on three types of 2D materials, namely graphene, h-BN, and MoS_2, each having different electronic properties. It was found that all of these 2D materials show Raman enhancement effects for the CuPc molecule but with different enhancement factors for different vibrational modes and different behaviors for different substrates. On both graphene and h-BN, the enhancement effect is obviously observed, while only a small enhancement effect was observed on MoS_2. Considering the electronic properties and polarity of graphene, h-BN, and MoS_2, we conclude that the strong charge transfer interaction between graphene and CuPc and the interface dipole−dipole interaction between h-BN and CuPc can induce an increase of the electron transition probability and consequently an enhancement of the Raman signal. Additionally, for MoS_2, both the charge transfer and interface dipole interaction are much weaker. This is why MoS_2 is expected to provide a weaker enhancement effect for this molecule in comparison to graphene and h-BN, in agreement with observation. This work confirms the importance of charge transfer for the Raman enhancement effect in a conducting substrate. Furthermore, we also demonstrate that the strong interface dipole−dipole interaction can also induce a significant Raman enhancement, such as for the CuPc molecule on an h-BN substrate. This study benefits the future potential application of 2D materials, as well as their hybrid structures, for their possible use in the observation and utilization of the SERS effect.

Experiment Section. *Preparation of Graphene, h-BN, and MoS_2.* In this work, graphene, h-BN, and MoS_2 are prepared by both mechanical exfoliation and CVD growth and transferred onto a cleaned 300 nm SiO_2/Si substrate. CVD graphene is synthesized on copper foil (99.9%, 127 μm thick, Alfa Aesar) using low-pressure chemical vapor deposition.[56] Before growth, the copper foil is annealed under 10 sccm hydrogen (~400 mTor) for 30 min. During growth, 1 sccm methane and 50 sccm hydrogen are introduced for 1 h (~1.5 mTor). After that, the copper foil is cooled down to room temperature under the same atmosphere. CVD h-BN is grown on an iron foil (99.99%, 0.1 mm thick, Alfa Aesar) using borazine as a precursor. The iron foil is first annealed for 1 h at 1100 °C under 100 sccm hydrogen and 100 sccm nitrogen at atmospheric pressure. Then the nitrogen gas is turned off and the process is switched to low pressure. Borazine is introduced by 0.15 sccm hydrogen as a carrier gas for 3 h. The iron foil is cooled down at 5 °C/min to 700 °C under the same atmosphere and followed by fast cooling to room temperature. MoS_2 was directly grown on the 300 nm SiO_2/Si substrate by using MoO_3 and sulfur as a precursor as reported.[57] For the graphene or h-BN transfer process, poly(methyl methacrylate) (PMMA, 4.5%) is spin coated on to the graphene/copper foil or h-BN/iron foil at 2500 rpm. The copper foil is etched using a copper etchant (CE-100, Transene Company Inc.) and the iron foil is removed by a nickel etchant (Nitric acid, Transene Company Inc.) After the graphene or h-BN film is transferred onto the SiO_2/Si substrate, the PMMA is removed by acetone vapor and thermal annealing at 350 °C for 2 h under 200 sccm hydrogen and 200 sccm argon.

Deposition of the CuPc and XPS Characterization. The CuPc molecule was deposited on the substrate by a standard thermal evaporator. The base pressure for deposition is about 1 × 10^{-6} Torr. The evaporation current is about 50 A. The deposition thickness of the CuPc molecule is monitored using a quartz crystal monitor. The typical thickness used is 2 and 4 Å, depending on different measurements. The amount of the CuPc molecules on the substrate is further characterized using the XPS technique. The XPS characterization was carried out using a Phi V5000 with an Al Ka X-ray source. The energy calibrations were made against the C 1s peak to eliminate the charging of the sample during analysis.

Raman measurement. The Raman measurement was carried out using a Horiba-Jobin Yvon system with a 633 nm He−Ne laser line and a 532 nm Ar+ laser line. The laser power used is around 1 mW on the sample and a 100× objective was used to focus. The size of the laser beam on the sample is around 1 μm. The typical spectral collection condition is a 10 s exposure time and a single accumulation. The comparison spectra in this work are collected under the same conditions. The obtained Raman signals are fitted by a Lorenzian function using the LabSpec software, and then the Raman shifts, intensity, full width at the half-maximum intensity are obtained.

UV−vis Absorption Measurement. For the UV−visible absorption measurement, the 2D materials were transferred by the PMMA method onto the quartz substrates, which are highly transparent (>95%) in the UV−vis range. The measurement was carried out on a Cary 500i UV−vis−NIR Dual-Beam Spectrophotometer using the transmission mode. The blank quartz substrate was used as a reference to remove the background. The spectrum range was typically from 175 to 800

nm. Typically, 4 Å of the CuPc molecule was deposited to measure the UV−vis absorption spectra.

■ ASSOCIATED CONTENT

Supporting Information

Assignment of the XPS signals; the Raman spectra of the CuPc (2 Å) molecule on the MoS_2 substrate without baseline correction; the Raman enhancement effect of the NAA molecule on graphene, h-BN, and MoS_2 substrates; the UV−vis absorption spectra of the CuPc molecules on a quartz substrate. This material is available free of charge via the Internet at http://pubs.acs.org.

■ AUTHOR INFORMATION

Corresponding Authors

*(M.S.D.) E-mail: millie@mgm.mit.edu. Tel: +1-617-253-6864.
*(X.L.) E-mail: xiling@mit.edu. Tel: +1-617-253-6864 (office); +1-617-583-3441 (home).

Notes

The authors declare no competing financial interest.

■ ACKNOWLEDGMENTS

This work is partially supported by the National Science Foundation under award number NSF/DMR 0845358, NSF/DMR 1004147, and National Natural Science Foundation of China under award number NSFC (21233001, 21129001)

■ REFERENCES

(1) Ferraro, J. R. *Introductory Raman Spectroscopy*; Academic Press: New York, 2003.
(2) Ferrari, A. C.; Robertson, J. *Phys. Rev. B* **2001**, *64*, 075414.
(3) Freudiger, C. W.; Min, W.; Saar, B. G.; Lu, S.; Holtom, G. R.; He, C.; Tsai, J. C.; Kang, J. X.; Xie, X. S. *Science* **2008**, *322*, 1857−1861.
(4) Campion, A.; Kambhampati, P. *Chem. Soc. Rev.* **1998**, *27*, 241−250.
(5) Nie, S.; Emory, S. R. *Science* **1997**, *275*, 1102−1106.
(6) Schatz, G. C.; Young, M. A.; Duyne, R. P. V. In *Surface-Enhanced Raman Scattering*; Kneipp, K., Moskovits, M., Kneipp, H., Eds.; Topics in Applied Physics; Springer: Berlin Heidelberg, 2006; pp 19−45.
(7) Wu, D.-Y.; Liu, X.-M.; Duan, S.; Xu, X.; Ren, B.; Lin, S.-H.; Tian, Z.-Q. *J. Phys. Chem. C* **2008**, *112*, 4195−4204.
(8) Yamada, H.; Nagata, H.; Toba, K.; Nakao, Y. *Surf. Sci.* **1987**, *182*, 269−286.
(9) Maitani, M. M.; Ohlberg, D. A. A.; Li, Z.; Allara, D. L.; Stewart, D. R.; Williams, R. S. *J. Am. Chem. Soc.* **2009**, *131*, 6310−6311.
(10) Otto, A. *J. Raman Spectrosc.* **2005**, *36*, 497−509.
(11) Xu, W.; Ling, X.; Xiao, J.; Dresselhaus, M. S.; Kong, J.; Xu, H.; Liu, Z.; Zhang, J. *Proc. Natl. Acad. Sci. U.S.A.* **2012**, *109*, 9281−9286.
(12) Hurst, S. J.; Fry, H. C.; Gosztola, D. J.; Rajh, T. *J. Phys. Chem. C* **2011**, *115*, 620−630.
(13) Musumeci, A.; Gosztola, D.; Schiller, T.; Dimitrijevic, N. M.; Mujica, V.; Martin, D.; Rajh, T. *J. Am. Chem. Soc.* **2009**, *131*, 6040−6041.
(14) Sun, Z.; Wang, C.; Yang, J.; Zhao, B.; Lombardi, J. R. *J. Phys. Chem. C* **2008**, *112*, 6093−6098.
(15) Ling, X.; Xie, L.; Fang, Y.; Xu, H.; Zhang, H.; Kong, J.; Dresselhaus, M. S.; Zhang, J.; Liu, Z. *Nano Lett.* **2010**, *10*, 553−561.
(16) Xu, W.; Mao, N.; Zhang, J. *Small* **2013**, *9*, 1206−1224.
(17) Ling, X.; Wu, J.; Xu, W.; Zhang, J. *Small* **2012**, *8*, 1365−1372.
(18) Zhu, X.; Shi, L.; Schmidt, M. S.; Boisen, A.; Hansen, O.; Zi, J.; Xiao, S.; Mortensen, N. A. *Nano Lett.* **2013**, *13*, 4690−4696.
(19) Heeg, S.; Fernandez-Garcia, R.; Oikonomou, A.; Schedin, F.; Narula, R.; Maier, S. A.; Vijayaraghavan, A.; Reich, S. *Nano Lett.* **2013**, *13*, 301−308.
(20) Khorasaninejad, M.; Raeis-Zadeh, S. M.; Jafarlou, S.; Wesolowski, M. J.; Daley, C. R.; Flannery, J. B.; Forrest, J.; Safavi-Naeini, S.; Saini, S. S. *Sci. Rep* **2013**, *3*, 2936.
(21) Fang, Z.; Liu, Z.; Wang, Y.; Ajayan, P. M.; Nordlander, P.; Halas, N. J. *Nano Lett.* **2012**, *12*, 3808−3813.
(22) Ling, X.; Zhang, J. *Small* **2010**, *6*, 2020−2025.
(23) Xu, H.; Xie, L.; Zhang, H.; Zhang, J. *ACS Nano* **2011**, *5*, 5338−5344.
(24) Hao, Q.; Morton, S. M.; Wang, B.; Zhao, Y.; Jensen, L.; Jun Huang, T. *Appl. Phys. Lett.* **2013**, *102*, 011102−011102−4.
(25) Ling, X.; Wu, J.; Xie, L.; Zhang, J. *J. Phys. Chem. C* **2013**, *117*, 2369−2376.
(26) Ling, X.; Moura, L. G.; Pimenta, M. A.; Zhang, J. *J. Phys. Chem. C* **2012**, *116*, 25112−25118.
(27) Sun, S.; Zhang, Z.; Wu, P. *ACS Appl. Mater. Interfaces* **2013**, DOI: 10.1021/am400938z.
(28) Ling, X.; Xie, L.; Fang, Y.; Xu, H.; Zhang, H.; Kong, J.; Dresselhaus, M. S.; Zhang, J.; Liu, Z. *Nano Lett.* **2010**, *10*, 553−561.
(29) Liu, L.; Feng, Y. P.; Shen, Z. X. *Phys. Rev. B* **2003**, *68*, 104102.
(30) Wang, Q. H.; Kalantar-Zadeh, K.; Kis, A.; Coleman, J. N.; Strano, M. S. *Nat. Nanotechnol.* **2012**, *7*, 699−712.
(31) Friend, R. H.; Yoffe, A. D. *Adv. Phys.* **1987**, *36*, 1−94.
(32) Shimada, T.; Hamaguchi, K.; Koma, A.; Ohuchi, F. S. *Appl. Phys. Lett.* **1998**, *72*, 1869−1871.
(33) Novoselov, K. S.; Geim, A. K.; Morozov, S. V.; Jiang, D.; Katsnelson, M. I.; Grigorieva, I. V.; Dubonos, S. V.; Firsov, A. A. *Nature* **2005**, *438*, 197−200.
(34) Geim, A. K.; Novoselov, K. S. *Nat. Mater.* **2007**, *6*, 183−191.
(35) Han, W.-Q.; Wu, L.; Zhu, Y.; Watanabe, K.; Taniguchi, T. *Appl. Phys. Lett.* **2008**, *93*, 223103−223103−3.
(36) Splendiani, A.; Sun, L.; Zhang, Y.; Li, T.; Kim, J.; Chim, C.-Y.; Galli, G.; Wang, F. *Nano Lett.* **2010**, *10*, 1271−1275.
(37) Ramprasad, R.; Shi, N. *Appl. Phys. Lett.* **2006**, *88*, 222903−222903−3.
(38) Bovill, A. J.; McConnell, A. A.; Nimmo, J. A.; Smith, W. E. *J. Phys. Chem.* **1986**, *90*, 569−575.
(39) Jiang, N.; Foley, E. T.; Klingsporn, J. M.; Sonntag, M. D.; Valley, N. A.; Dieringer, J. A.; Seideman, T.; Schatz, G. C.; Hersam, M. C.; Van Duyne, R. P. *Nano Lett.* **2012**, *12*, 5061−5067.
(40) Tackley, D. R.; Dent, G.; Smith, W. E. *Phys. Chem. Chem. Phys.* **2001**, *3*, 1419−1426.
(41) Ling, X.; Zhang, J. *Acta Phys.−Chim. Sin.* **2012**, *28*, 2355−2362.
(42) Yaghobian, F.; Korn, T.; Schüller, C. *ChemPhysChem* **2012**, *13*, 4271−4275.
(43) Xiao, K.; Deng, W.; Keum, J. K.; Yoon, M.; Vlassiouk, I. V.; Clark, K. W.; Li, A.-P.; Kravchenko, I. I.; Gu, G.; Payzant, E. A.; Sumpter, B. G.; Smith, S. C.; Browning, J. F.; Geohegan, D. B. *J. Am. Chem. Soc.* **2013**, *135*, 3680−3687.
(44) Bonaccorso, F.; Sun, Z.; Hasan, T.; Ferrari, A. C. *Nat. Photonics* **2010**, *4*, 611−622.
(45) Bruna, M.; Borini, S. *Appl. Phys. Lett.* **2009**, *94*, 031901−031901−3.
(46) Rana, F. *IEEE Trans. Nanotechnol.* **2008**, *7*, 91−99.
(47) Marom, N.; Hod, O.; Scuseria, G. E.; Kronik, L. *J. Chem. Phys.* **2008**, *128*, 164107.
(48) Aristov, V. Y.; Molodtsova, O. V.; Maslyuk, V.; Vyalikh, D. V.; Zhilin, V. M.; Ossipyan, Y. A.; Bredow, T.; Mertig, I.; Knupfer, M. *Appl. Surf. Sci.* **2007**, *254*, 20−25.
(49) Liao, M.-S.; Scheiner, S. *J. Comput. Chem.* **2002**, *23*, 1391−1403.
(50) Xiao, K.; Liu, Y.; Huang, X.; Xu, Y.; Yu, G.; Zhu, D. *J. Phys. Chem. B* **2003**, *107*, 9226−9230.
(51) Tian, M.; Yanagi, S.; Sasaki, K.; Wada, T.; Sasabe, H. *J. Opt. Soc. Am. B* **1998**, *15*, 846−853.
(52) Alexiou, M. S.; Tychopoulos, V.; Ghorbanian, S.; Tyman, J. H. P.; Brown, R. G.; Brittain, P. I. *J. Chem. Soc., Perkin Trans. 2* **1990**, 837−842.
(53) Basova, T.; Kol'tsov, E.; Hassan, A.; Tsargorodskaya, A.; Ray, A.; Igumenov, I. *Phys. Status Solidi B* **2005**, *242*, 822−827.

(54) Liu, W.; Priddy, T. S.; Carlson, G. M. *Protein Sci.* **2008**, *17*, 2111−2119.
(55) Basova, T. V.; Kiselev, V. G.; Schuster, B.-E.; Peisert, H.; Chassé, T. *J. Raman Spectrosc.* **2009**, *40*, 2080−2087.
(56) Fang, W.; Hsu, A. L.; Caudillo, R.; Song, Y.; Birdwell, A. G.; Zakar, E.; Kalbac, M.; Dubey, M.; Palacios, T.; Dresselhaus, M. S.; Araujo, P. T.; Kong, J. *Nano Lett.* **2013**, *13*, 1541−1548.
(57) Lee, Y.-H.; Zhang, X.-Q.; Zhang, W.; Chang, M.-T.; Lin, C.-T.; Chang, K.-D.; Yu, Y.-C.; Wang, J. T.-W.; Chang, C.-S.; Li, L.-J.; Lin, T.-W. *Adv. Mater.* **2012**, *24*, 2320−2325.